Strength analysis and failure prediction of thin tow-based discontinuous composites

Downloaded from: https://research.chalmers.se, 2026-04-04 21:27 UTC

Citation for the original published paper (version of record):
Katsivalis, I., Persson, M., Johansen, M. et al (2024). Strength analysis and failure prediction of thin tow-based discontinuous composites. Composites Science and Technology, 245. http://dx.doi.org/10.1016/j.compscitech.2023.110342

N.B. When citing this work, cite the original published paper.

research.chalmers.se offers the possibility of retrieving research publications produced at Chalmers University of Technology. It covers all kind of research output: articles, dissertations, conference papers, reports etc. since 2004. research.chalmers.se is administrated and maintained by Chalmers Library

(article starts on next page)

Composites Science and Technology 245 (2024) 110342

Contents lists available at ScienceDirect

Composites Science and Technology

journal homepage: www.elsevier.com/locate/compscitech

Strength analysis and failure prediction of thin tow-based discontinuous composites

Ioannis Katsivalis [a,*], Mattias Persson [a], Marcus Johansen [a], Florence Moreau [b], Erik Kullgren [c], Monica Norrby [d], Dan Zenkert [d], Soraia Pimenta [e], Leif E. Asp [a]

[a] Department of Industrial and Materials Science, Chalmers University of Technology, Sweden
[b] Oxeon AB, Sweden
[c] Elitkomposit AB, Sweden
[d] Department of Engineering Mechanics, KTH, Sweden
[e] Department of Mechanical Engineering, Imperial College London, UK

ARTICLE INFO

Handling Editor: Marino Quaresimin

Keywords:
Short-fibre composites
Interfacial strength
Elastic properties
Scanning electron microscopy (SEM)
Compression moulding

ABSTRACT

Tow Based Discontinuous Composites (TBDCs) are a new class of composite materials which combine in-plane isotropy, high strength and stiffness and enhanced manufacturability. However, due to their complicated micro-architecture, characterising the performance of these materials and predicting their response is challenging. This work develops a complete experimental and analytical framework which identifies all the key properties in the performance of the TBDCs, characterises them experimentally and builds an analytical predictive tool for both the stiffness response and the strength of the TBDC material. Fractography is also utilised to identify the damage mechanisms and correlate them with the analytical predictions. A parametric study is developed which shows the critical effect that the tape thickness and mode II fracture toughness have on the TBDCs. Finally, the performance of the material is compared to similarly developed TBDCs from the literature and shows the significant strength and stiffness increases recorded through the combination of the thin high-modulus tapes and the increased fibre volume fractions.

1. Introduction

Nacre, or the mother of pearl, is one of the most efficient composite materials found in nature. Nacre utilises a brick-mortar structure combining stiff platelets with a soft matrix. Inspired from nacre, discontinuous composites are a new class of materials which gained interest over the last years as they offer significant advantages over conventional composites. Takahashi and co-workers have shown the potential of manufacturing quasi-isotropic composite materials from randomly distributed CFRP tapes [1–3].

Compared to continuous-fibre composites, Tow Based Discontinuous Composites (TBDCs) can a) utilise unconventional micro-architectures allowing for random fibre orientation leading to in-plane quasi-isotropic performance, b) increase the attainable fibre volume fractions leading to increased strength and c) provide enhanced manufacturability. Therefore, TBDCs expand the design space of fibre reinforced composites significantly [4].

Discontinuous tape-based composites can be used in several applications where high volumes and complex shapes are required. There is a particular interest for instance, in the automotive industry [5]. The tape structure of the material is maintained after press-forming as the flow distances are very limited and complex shapes can be achieved as the short thin tapes slide relative to each other during preform draping, as suggested in a recent review by Wan and Takahashi [5]. This does potentially allow for use of high modulus fibres in highly curved structures, something that cannot be achieved by continuous fibre composites as the fibres will break [4]. Thus, the moulding flexibility of this type of composite does not rely on the flowing of the thin tapes, or the pre-impregnated resin, but rather on the sliding between the tapes. To achieve this, preforms of randomly distributed thin tapes are prepared and shaped prior to consolidation and cure or solidification.

The stiffness and strength prediction along with the damage and failure mechanisms of these materials is less straightforward. FE methods have been used to predict the response of TBDC materials. For instance, Chen et al. [6] used a Representative Volume Element (RVE) model, considered damage in the fibre, the matrix and the interface and

* Corresponding author.
E-mail address: ioannis.katsivalis@chalmers.se (I. Katsivalis).

https://doi.org/10.1016/j.compscitech.2023.110342
Received 10 May 2023; Received in revised form 30 October 2023; Accepted 2 November 2023
Available online 7 November 2023
0266-3538/© 2023 The Authors. Published by Elsevier Ltd. This is an open access article under the CC BY license (http://creativecommons.org/licenses/by/4.0/).

managed to achieve good agreement between numerical predictions and experimental observations. Li et al. [7] reconstructed the TBDC microstructure numerically and developed an FE model which utilises the material processing information to predict the mechanical properties of the composite. More recently, Alves et al. [8] demonstrated significant strength prediction improvements by integrating process simulation results to a 3D FE stochastic network as compared to a deterministic FE approach.

FE methods are computationally expensive and thus the development of analytical solutions with the ability to capture the strength and stiffness of TBDC materials has been an active field of research. Li et al. [9] compared the strength and stiffness responses of TBDCs and their equivalent laminates and confirmed experimentally that the equivalent laminate assumption can be used for stiffness predictions. The comparison was based on two different tow thicknesses and showed that the equivalent laminate assumption can predict the failure mechanisms of TBDCs but is less accurate in strength predictions. It was also noted that the heterogeneity of the TBDC materials introduces microstructural variability and thus lower strengths compared to the equivalent laminates.

Pimenta and Robinson [10] developed an analytical shear lag model to predict the tensile response of discontinuous composites assuming a simple brick-mortar architecture. Two important parameters in the model definition are the absolute thickness of the tow and the tow aspect ratio. For relatively low tape aspect ratios and high matrix ductility, the strength of the composite is driven by the development of matrix plasticity during the transfer of shear stresses between the tows; therefore, in this case the composite strength depends on the tape aspect ratio and the shear strength of the matrix. However, when the matrix is more brittle, or for thicker tows with larger aspect ratios, the damage mechanism is governed by a shearing fracture mechanism and, therefore, the mode II interfacial fracture toughness has a strong effect on the strength of the TBDC.

The use of thin plies is also known to improve the performance of composite materials especially relating to their strength [11]. This is achieved by delaying or even supressing matrix cracking and free edge delamination and promoting fibre related failure mechanisms [12]. Li and Pimenta [13] predicted the tow thickness effect on the strength of TBDCs by using analytical methods based on the brick-mortar architecture assumption. The finite value of the fibre/matrix interfacial shearing fracture toughness was shown to play a significant role in the shear-lag formulation.

Alves et al. [4] investigated experimentally and numerically the effect of the tow thickness and fibre stiffness on the response of TBDCs. An initial parametric study revealed that ultra-thin (20 μm) and high modulus (425 GPa) carbon fibre tapes can be used to manufacture TBDCs with at least the strength and stiffness of quasi-isotropic laminates and therefore expand the design space even further. Experimentally, the authors used resin films for the TBDC manufacturing which led to relatively low fibre volume fractions. Therefore, the authors linearly scaled up the strength and stiffness values achieved with the fibre volume fraction to allow for direct comparisons amongst the materials produced within their work and across the literature.

A complete experimental and analytical framework for the property characterisation and performance prediction of thin-ply TBDCs is currently lacking. This work provides a detailed experimental and analytical investigation on the performance of thin-ply discontinuous composites. The critical parameters for the stiffness and strength prediction were identified and extracted experimentally, an analytical model was developed which considered different damage mechanisms and finally the model predictions were validated by comparison with tensile testing on discontinuous thin-ply composites. The continuum-based analytical approach presented here is complementary to the more complex and detailed stochastic numerical models developed in the past by Pimenta and co-authors [8], and provides an additional, easy-to-use, fully analytical method with the ability to estimate the strength and stiffness of TBDC materials. It is worth highlighting that the absolute value of the achieved tensile strength was about 30% higher than any TBDC material system reported in the past due to the micro-architecture and the high fibre volume fractions attained.

2. Materials and methods

2.1. Plate manufacturing

An experimental campaign was designed to characterise a) the properties of the thin tapes under tension, b) the thin-ply interlaminar fracture toughness under mode II and c) the response of the TBDC material under tensile loading. Three types of 300 × 300 mm plates were manufactured for each of the tests described in Sections 2.2, 2.3 and 2.4. Fig. 1 shows details of the plates manufactured and the specimen positions while Fig. 2 shows one of the manufactured TBDC plates and characteristic examples of the specimens tested. In addition, Supplementary Fig. S1 provides a micrograph of the cross section of the TBDC material highlighting the lack of resin rich areas with the current manufacturing process.

The tapes were produced by TeXtreme® Spread Tow technology at the facilities of Oxeon AB, using Pyrofil$_{TM}$ MR70 12P carbon fibre from Mitsubishi Chemical Carbon Fiber and Composites. The modulus of the fibres used was 325 GPa and strength was 7000 MPa. The tape was 20 mm wide leading to a fibre areal weight of 21 gsm. The tapes were partially impregnated at Oxeon AB with an epoxy resin curing at 150 °C to reach a 35%w resin content leading to a theoretical cured ply thickness of 0.0214 mm. The manufacturing of the preforms for all plates was done at Oxeon AB.

For the UD plate, a winding equipment was used to unwind the TeXtreme tapes and generate the thin plies. Afterwards, each ply was placed and stacked on top of each other to create the UD preform.

For the TBDC plate, the continuous impregnated tapes were cut and placed using an automated process on a supporting carrier at random locations and orientations. The tape pieces were 20 mm wide and 40 mm long. The amount of tape used was determined according to the desired cured ply thickness of the TBDC sheet. Slight pre-consolidation of the sheets was done at room temperature for better handleability. The 300 × 300 mm preforms were cured with press moulding according to the following cycle. Initially, the temperature was ramped up to 120 °C and a dwell time followed for 10 min. Afterwards, the temperature ramp continued to 150 °C with a dwell time of another 10 min. The temperature was maintained at 150 °C for 90 min and the pressure applied was 20 bar. Finally, the plates were cooled down to 50 °C before removing the pressure and demoulding. It is worth noting that the presented TBDC methodology is better suited for applications where high fibre volume fractions are achieved and tape flow is restricted.

2.2. UD tensile testing

The UD tensile testing was conducted according to ASTM D3039 [14] in order to extract the in-plane elastic properties of the tapes. Tests were conducted in both the fibre (0°) and the transverse (90°) direction as shown in Fig. 1a. 300 × 300 mm plates were manufactured with a thickness of 0.35 mm and 150 × 15 mm specimens were cut from these plates. To ensure sufficient gripping of the specimens, GFRP end tabs were bonded to the specimens. A universal servo-hydraulic loading machine was used, and the loading rate was adjusted to 1 mm/min for the 0° orientation specimens while 0.25 mm/min was used for the 90° orientation specimens ensuring that the total duration of each test was 5–10 min. The full field strain was monitored with a stereo DIC system and virtual extensometers were used to extract the longitudinal and transverse strains. The camera resolution was 2448 × 2050 pixels, the subset size was 40 pixels while the subset step was 20 pixels. A minimum of 5 specimens was tested per direction.

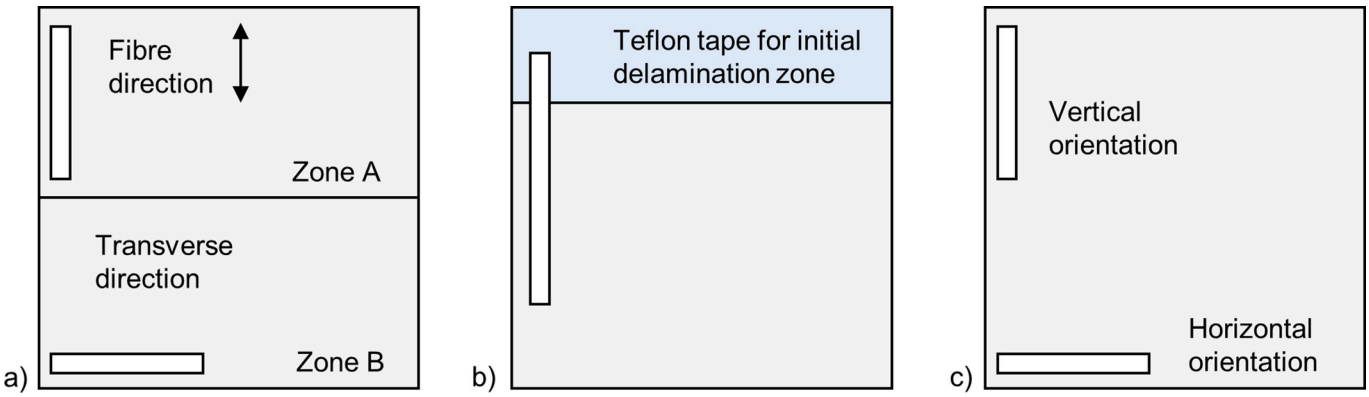

Fig. 1. Detail of the plate and the specimen locations for the a) UD testing, b) mode II fracture toughness testing and c) TBDC testing.

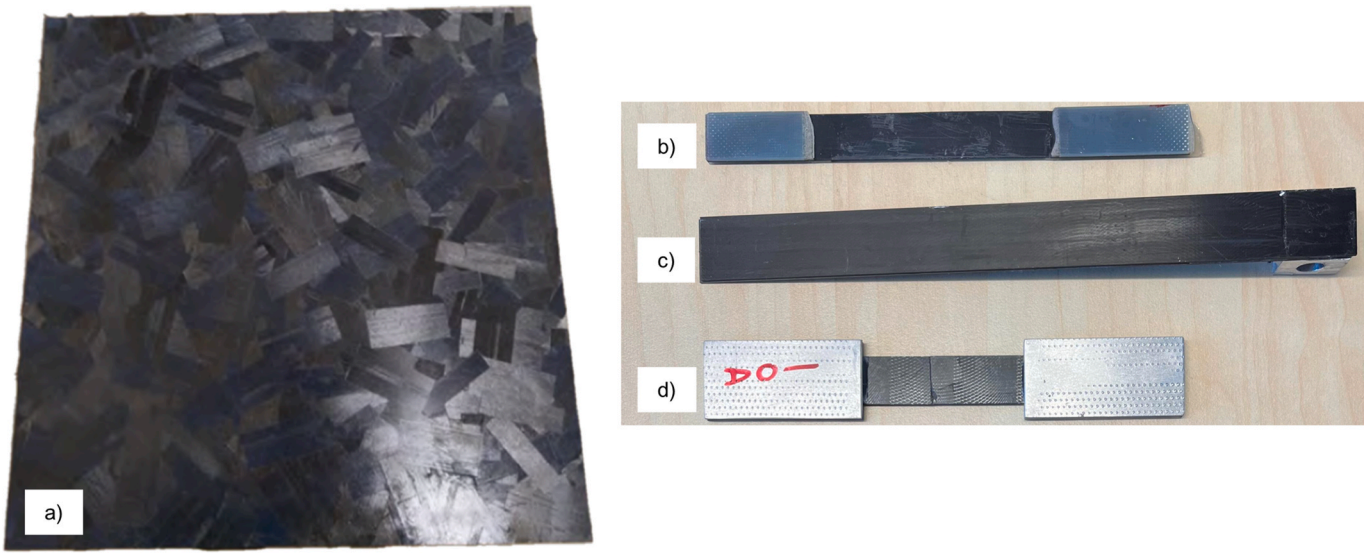

Fig. 2. a) Characteristic TBDC plate manufactured and specimens used for the a) UD testing, b) mode II fracture toughness testing and c) TBDC testing.

2.3. Mode II ELS testing

The mode II testing was conducted according to ISO 15114-2014 [15] in order to extract the interlaminar fracture toughness of the thin tapes under shear loading. The End-Loaded Split (ELS) specimens consisted of thick UD plies (134 gsm) in the two arms while thin plies (21 gsm) were introduced in the interface region. A small angle was also introduced in the thin interfacial plies $[+5^\circ/\text{-}5^\circ/]_2$ to define a distinct interface and prevent fibre bridging. This method has been used in the literature and was validated by Juntti et al. [16] showing no significant effects on the measured interfacial fracture toughness. Teflon tape was used between the $+5^\circ$ and -5° plies for crack initiation (Fig. 1b). 300 × 300 mm plates with a total thickness of 3 mm were manufactured, and 200 × 20 mm specimens were cut for the mode II testing.

A compliance calibration was initially performed which considers the flexural stiffness of the specimen and the compliance of the loading machine. Afterwards, a mode II pre-crack was generated on the specimens and finally the mode II testing was performed. Supplementary Fig. 2 shows the mode II testing experimental setup and provides a sketch of the experimental setup with testing details. A universal servo-electrical loading machine was used, and the loading rate was set to 0.5 mm/min while the free length was adjusted to ensure stable crack propagation. A rolling table was also used to ensure the correct alignment and positioning of the specimen. The loading/displacement curve was recorded during the loading and unloading stages while a minimum of 5 specimens were tested.

The interlaminar fracture toughness was calculated based on the corrected beam theory as shown in equation (1) using the effective crack length as shown in equation (2).

$$G_{IIc} = \frac{9P^2a_e^2}{4b^2h^3E_1} \tag{1}$$

$$a_e = \left[\frac{1}{3}\left\{2bCh^3E_1 - \left(L + \Delta_{clamp}\right)^3\right\}\right]^{\frac{1}{3}} \tag{2}$$

In equation (1), P is the load applied, a_e is the effective crack length, b and h are the width and thickness of each arm respectively, and E_1 is the flexural modulus of the specimen. In equation (2), C is the compliance, L is the free length and Δ_{clamp} is the clamp correction. The values for the flexural modulus E_1 and the clamp correction Δ_{clamp} were determined during the compliance calibration. After the testing, the fracture surfaces were also examined using Scanning Electron Microscopy (SEM).

2.4. TBDC tensile testing

The tensile testing of the TBDC material was also based on ASTM D3039 [14]. The purpose of this test was to characterise the performance of the TBDC under tension in terms of stiffness, strength and strain to failure. In addition, the damage mechanisms were identified and compared with the analytical predictions. 300 × 300 mm plates

were manufactured with a thickness of 1.5 mm and 150 × 15 mm specimens were cut from these plates. Two specimen orientations were used to validate the quasi-isotropic performance of the TBDCs as shown in Fig. 1c. To ensure sufficient gripping of the specimens, aluminium end tabs were bonded to the specimens. A universal servo-hydraulic loading machine was used, and the loading rate was adjusted to 1 mm/min while the full field strain was monitored with a stereo DIC system. The camera resolution was 2448 × 2050 pixels, the subset size was 40 pixels while the subset step was 20 pixels. A total of 8 specimens was tested. The specimens were examined with SEM after testing to identify the damage and failure mechanisms through fractography. The results of these tests were also used to validate the analytical models developed.

2.5. SEM analysis

SEM was used to examine the fracture surfaces for the ELS and the TBDC specimens. Characteristic surfaces were cut from the failed specimens and were mounted on stubs. Afterwards, a thin layer of about 5 μm of gold sputter was applied to the specimens and those were examined with a JEOL 7800F Prime. The microscope magnifications used were in between × 500 and × 8000 with an acceleration voltage of 5 kV.

2.6. Fibre volume fraction

The fibre volume fraction of the UD and TBDC plates was determined by performing matrix digestion in nitric acid according to ASTM D3171 [17]. The total mass of the composite m_c was measured before the exposure to the nitric acid. After the exposure, the mass of the fibres m_f was measured and the fibre volume fraction V_f was calculated based on the densities of the fibres ρ_f and the matrix ρ_m, according to equation 3

$$V_f = \frac{1}{1 + \frac{\rho_f}{\rho_m}\left(\frac{m_c}{m_f} - 1\right)} \tag{3}$$

3. Analytical model

3.1. Stiffness prediction

The Equivalent Laminate Theory (ELT) was used to calculate the global stiffness of the TBDC material and the tape stiffness as a function of the tape angle. An equivalent quasi-isotropic laminate with 8 total plies $[0,45,-45,90]_s$ was assumed and the calculations which were based on [9] can be found in the supplementary information. In addition, for simplicity, the in-plane modulus $\overline{E}_x$ for a randomly oriented composite can be approximated as shown in equation (4). The tape modulus was given as a function of the angle as shown in equation (5). It is worth noting that a 0° angle stands for a tape oriented in the load direction while a 90° angle stands for a tape oriented perpendicular to the load direction. In equations (4) and (5), E_L, E_T, G_{LT} are the longitudinal, transverse and shear moduli while ν_{LT} is the major longitudinal Poisson's ratio of the tapes.

$$\overline{E}_x = \frac{3}{8}E_L \tag{4}$$

$$E_{tape(\theta)} = \frac{1}{\frac{cos^4(\theta)}{E_L} + \frac{sin^4(\theta)}{E_T} + \frac{sin^2(\theta)}{4}\left(\frac{1}{G_{LT}} - 2\frac{\nu_{LT}}{E_L}\right)}, 0° \leq \theta \leq 90° \tag{5}$$

3.2. Tape fracture

The Hashin failure criteria [18] were used to predict tape fracture in the TBDC. More specifically, strain expressions for the fibre and matrix dominated fractures are given in equations (6) and (7)

$$\varepsilon_1^D = \sqrt{\left(\frac{\varepsilon_{11}}{X_e}\right)^2 + \left(\frac{\gamma_{12}}{\varepsilon_{s,is}^T}\right)^2} \tag{6}$$

$$\varepsilon_2^D = \sqrt{\left(\frac{\varepsilon_{22}}{\varepsilon_{Y,is}^T}\right)^2 + \left(\frac{\gamma_{12}}{\varepsilon_{s,is}^T}\right)^2} \tag{7}$$

In equations (6) and (7), ε_{11}, $\varepsilon_{22}, \gamma_{12}$ are the normal and shear in-plane strains respectively, while X_e is the strain to the failure of the fibres. In addition, $\varepsilon_{Y,is}^T$ and $\varepsilon_{s,is}^T$ are the in-situ transverse tensile and shear strains to failure respectively, as adopted by Camanho et al. [19]. It is worth noting that there are linear and non-linear expressions for both strains. In this work, the linear case was adopted being more conservative. In addition, considering that the outer thin plies typically fail earlier, the outer thin ply assumption was considered as more conservative for our study. Therefore, the in-situ transverse tensile strain and the in-situ shear strain were given by equations (8) and (9) respectively

$$\varepsilon_{Y,is}^T = \frac{1}{E_{tape}(\theta)}\sqrt{\frac{8G_{Ic}}{\pi t_{tape}\Lambda_{22}^{\circ}}} \tag{8}$$

$$\varepsilon_{s,is}^T = \frac{2}{G_{LT}}\sqrt{\frac{G_{LT}G_{IIc}}{\pi t_{tape}}} \tag{9}$$

In equations (8) and (9), t_{tape} is the tape thickness, G_{Ic} and G_{IIc} are the values of fracture toughness in modes I and II respectively, and finally, the term Λ_{22}° was given as shown in equation 10

$$\Lambda_{22}^{\circ} = 2\left(\frac{1}{E_T} - \frac{\nu_{LT}^2}{E_L}\right) \tag{10}$$

Utilising the transformation matrices and setting as damage initiation criteria for longitudinal and transverse tape fracture, $\varepsilon_1^D = 1$ and $\varepsilon_2^D = 1$, equations (6) and (7) were expressed as shown in equations (11) and (12)

$$\varepsilon_{tape,L} = \frac{1}{\sqrt{\frac{cos^4(\theta)}{X_e^2} + \frac{4\ sin^2(\theta)cos^2(\theta)}{\left(\varepsilon_{S,is}^T\right)^2}}} \tag{11}$$

$$\varepsilon_{tape,T} = \frac{1}{\sqrt{\frac{sin^4(\theta)}{\left(\varepsilon_{Y,is}^T\right)^2} + \frac{4\ sin^2(\theta)cos^2(\theta)}{\left(\varepsilon_{S,is}^T\right)^2}}} \tag{12}$$

3.3. Tape pull-out

Tape pull-out is controlled by a fracture mechanics related process during which a mode II crack extends between the tow interfaces. The damage is assumed to initiate at the ends of the tows and moving inwards and in addition, the effects of friction are neglected [10]. The overall strength of the composite is thus controlled by the stiffness of the tows, the mode II interfacial fracture toughness of the composite and the absolute value of the tow thickness as shown in equation 13

$$\varepsilon_{pull-out} = \frac{1}{\overline{E}_x}\sqrt{\frac{2E_{tape(\theta)}G_{IIc}}{t_{tape}}} \tag{13}$$

4. Results

4.1. UD stiffness and strength

Fig. 3a shows the stress/strain curves in the fibre direction while Fig. 3b shows the stress/strain curves in the transverse direction. Table 1 summarises the elastic properties extracted from the tensile testing.

It is worth noting that the manufactured plate had small thickness

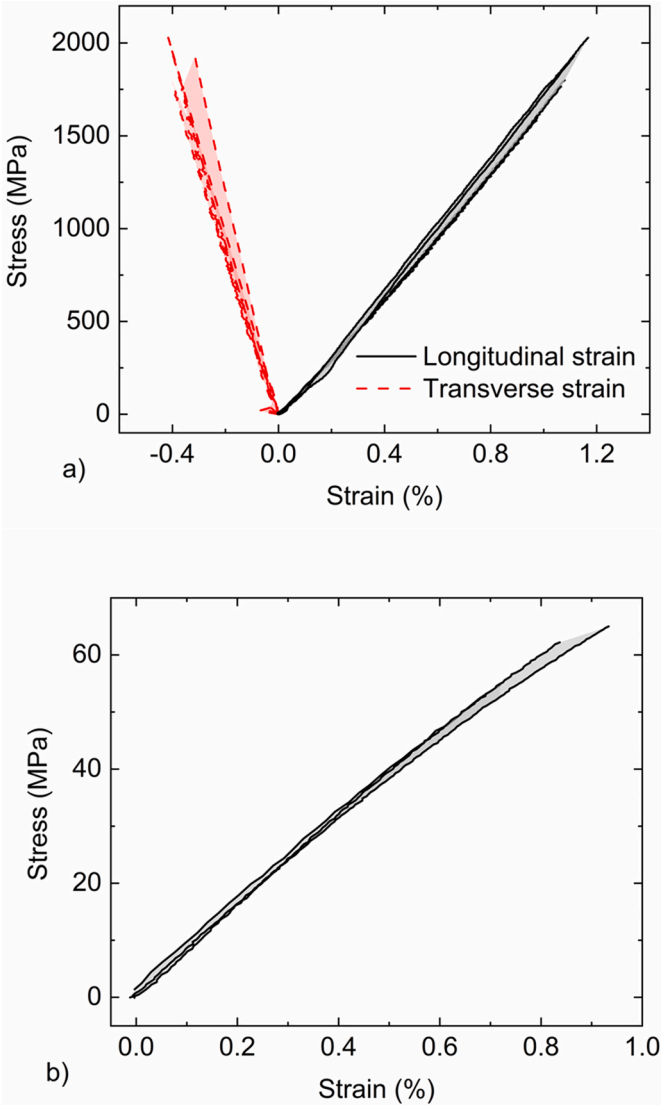

Fig. 3. Stress strain curves for the tensile testing of the UD tapes in (a) the fibre and (b) the transverse direction.

Table 1
Measured and estimated material properties of the UD and randomly distributed discontinuous composite materials.

Property	Symbol	Value	Units
Tape longitudinal modulus[a]	E_L	172 ± 5	(GPa)
Tape transverse modulus[a]	E_T	8.11 ± 0.05	(GPa)
Tape Poisson's ratio[a]	ν_{LT}	0.35 ± 0.03	(−)
Tape shear modulus[b]	G_{LT}	2.98	(GPa)
Fibre strain-to-failure[c]	X_e	2.2	(%)
Tape thickness[c]	t_{tape}	0.0214	(mm)
Mode II fracture toughness[a]	G_{IIc}	494 ± 20	(J/m^2)
TBDC in-plane modulus[d]	$\overline{E}_x$	70.0	(GPa)
TBDC in-plane Poisson's ratio[d]	ν	0.33	(−)

[a] Measured experimentally.
[b] Calculated analytically based on the Halpin-Tsai formulation and assuming isotropic fibres and fibre Poisson's ratio of 0.25.
[c] Values provided by the supplier.
[d] Calculated based on normalised values and the Equivalent Laminate Theory (ELT).

differences which indicate slightly different fibre volume fractions across different locations. For the thicker part of the plate (zone A as shown in Fig. 1a), the thickness was about 0.39 mm, and the fibre volume fraction was measured as 54.7% while for the thinner part of the plate (zone B as shown in Fig. 1a) the thickness was 0.36 mm, and the fibre volume fraction was estimated as 60.1%. The fibre volume fraction of the TBDC was measured as 59.4% and therefore the extracted longitudinal and transverse properties of the UD were normalised to match the TBDC fibre volume fraction.

4.1.1. Tape properties

Based on the ELT formulations (section 3.1), the UD stiffness results (section 4.1), and the measured fibre volume fractions (section 4.1) the in-plane tape and TBDC properties were determined as shown in Table 1. In addition, Table 1 also provides, the parameters needed for the analytical model presented in section 3.

4.2. Mode II fracture toughness

Fig. 4a shows the compliance curves extracted for different free lengths of the ELS specimen while Fig. 4b plots the compliance values against the free length of the specimen. Fig. 4b thus allows to extract the

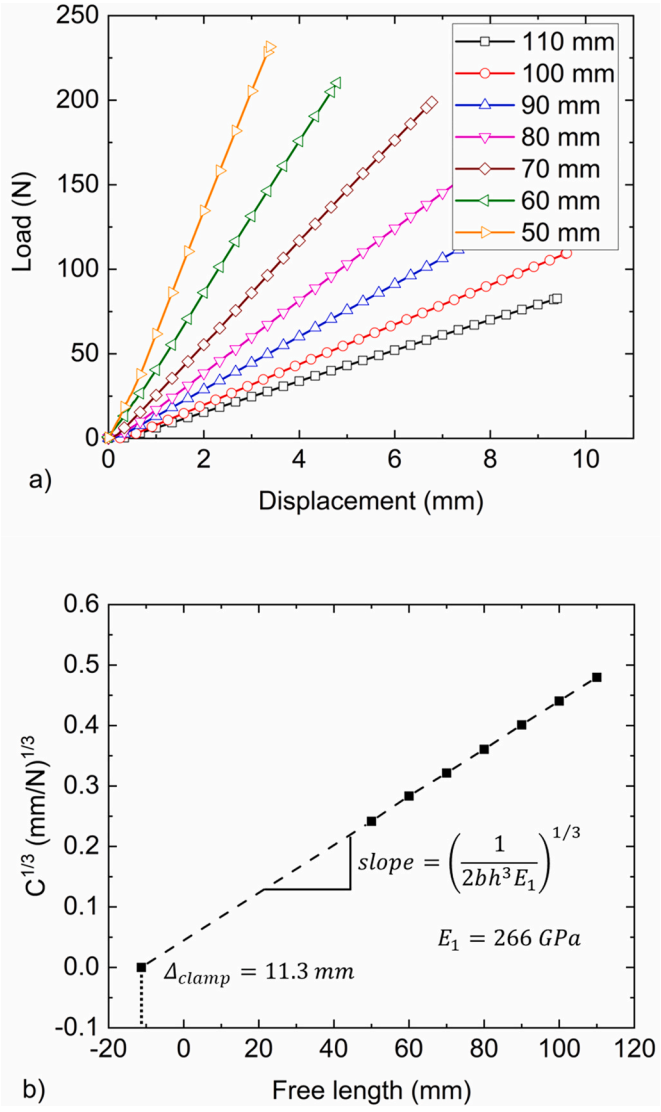

Fig. 4. a) Load displacement curves for different values of the free length of the ELS specimen and b) Compliance calibration against the free specimen length.

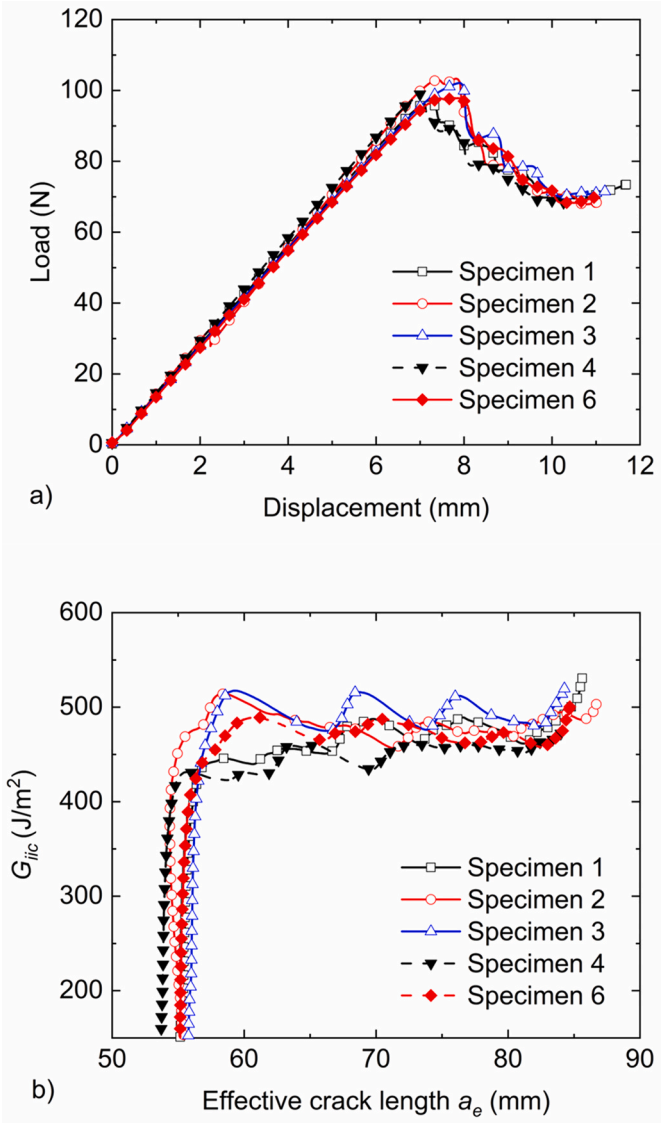

Fig. 5. a) Load-displacement curves and b) mode II fracture toughness against effective crack length for the ELS specimens.

flexural stiffness of the specimen and the clamp correction factor.

Fig. 5a shows the load displacement curves for the tested specimens while Fig. 5b plots the R-curves for the same specimens. There was small variability in the stiffness, the damage initiation load, and the slope in the damage propagation region. Stable crack propagation was ensured and the average value of the fracture toughness for all specimens was $494 \pm 20\ J/m^2$.

This measured mode II toughness is relatively low compared to that of composites typically used in aerospace applications. Fig. 6a shows a general overview of the damage detected using SEM, where the characteristic mode II failure cusps are displayed. Fig. 6b shows the residual matrix porosity on a fibre, which can partly explain the relatively low value of the interfacial fracture toughness extracted during mode II testing.

4.3. Tensile testing of TBDC

Fig. 7 shows the full field longitudinal strain in one of the TBDC specimens as the tensile loading was increasing. A stress concentration developed in the bottom of the specimen where the longitudinal strain peaked before failure. Similar locations were identified in all specimens. However, the average strain in the gauge section was monitored with a longitudinal and a horizontal virtual extensometer and Fig. 8 shows the extracted stress/strain curves for all TBDC specimens tested. The vertical and horizontal annotations in the plot indicate the orientation of the specimens relative to their position in the plate as shown in Fig. 1c, while the ε_x and ε_y annotations stand for the longitudinal and transverse strains respectively. The in-plane elastic modulus of the specimens was calculated as 69.9 GPa while Poisson's ratio was estimated as 0.36. In addition, the average strength of the specimens reached 674 MPa while the strain to failure was 0.97%. The specimens displayed linear behaviour until failure and there was no significant difference in the performance between specimens with different orientations, thereby validating the in-plane isotropy assumption.

Fig. 9 shows the macroscopic and microscopic damage mechanism observed in the TBDC specimen after failure. On the macroscopic scale as shown in Fig. 9a and b, different damage mechanisms can be observed including fibre fracture and tape pull-out. However, these figures do not provide conclusive outcomes regarding the initiating damage mechanism. The microscopic analysis (Fig. 9d) however reveals the presence of mode II cusps, similar to the ones observed during the ELS testing (Fig. 9c), indicating the presence of shear fracture in the tape interfaces leading to pull-out.

4.4. Analytical predictions

The analytical model described in Section 3 was used to predict the stiffness response and the damage load and mechanism of TBDC specimens under tensile load. Fig. 10 plots the strain to failure against the tape orientation angle. It is shown that the damage mechanism makes a

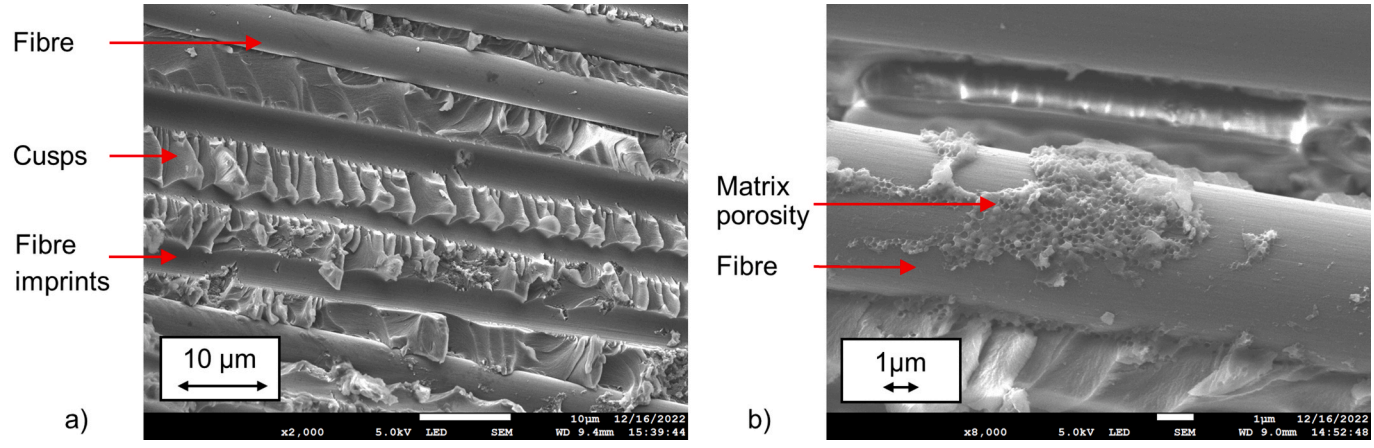

Fig. 6. a) Shear cusps developing on the delamination interface due to mode II fracture and b) matrix microporosity identified using SEM.

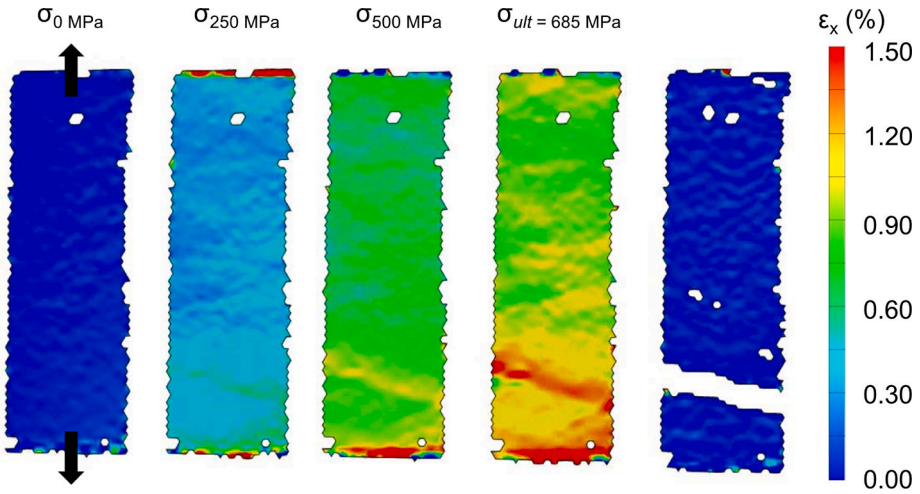

Fig. 7. Full field strain distribution in a characteristic TBDC specimen with increasing tensile loading.

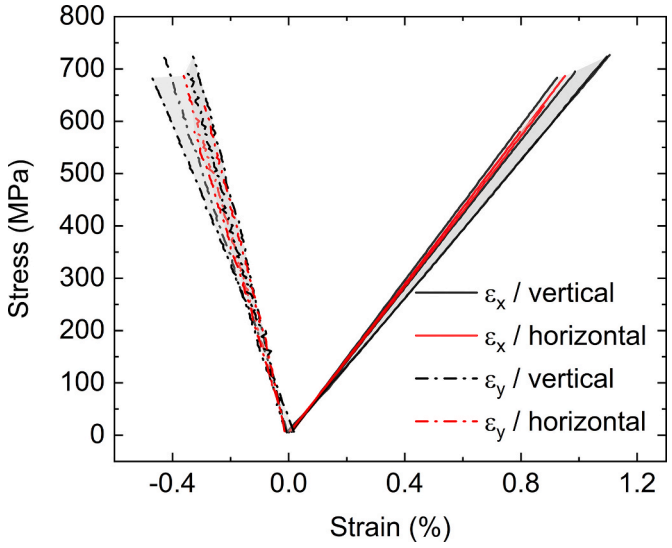

Fig. 8. Stress strain response of the TBDC material under tensile loading. The vertical and horizontal annotations stand for the position of the specimen in the plate while the ε_x and ε_y stand for the longitudinal and transverse strains respectively.

transition at about 12° from longitudinal tape fracture to tape pull-out, which is the dominant mode of failure for all other tape orientations. It is worth noting that due to the completely random orientation of the tapes, all possible tape angles are expected to be found in every single specimen. Therefore, the failure criterion assumed in this work is based on the minimum failure strain as a function of the tape orientation angle which is expected to lead to the failure of the entire TBDC specimen. Fig. 10 highlights the lowest strain value of every tape orientation angle and the strain triggering damage initiation which is found at a tape with an angle of 60°.

It is worth noting that there is some discrepancy between the model predictions for the unique case of 0° tape orientation which corresponds to the UD case. The analytical prediction for the longitudinal tape fracture is based on the fibre strain to failure value as provided by the fibre supplier (Table 1). However, in practice, the strength of CFRP is governed by the largest defect, also known as volume effect and thus the thick UD composite is expected to have a lower strain-to-failure compared to the single ply. Therefore, for the case of the 0° tape orientation, the model overestimates the tape strain-to-failure which is expected to be found between the failure strain of the individual fibres and the UD specimens.

5. Discussion and conclusions

5.1. Agreement between analytical method and experiments

Table 2 compares the analytical predictions with the experimental measurements from the tensile tests of the TBDC in terms of stiffness, strength, strain to failure, and failure mechanism. The analytical solution predicts the failure mechanism as tape pull-out; the presence of this mechanism was confirmed by the SEM analysis presented in Section 4.3. In addition, the analytical model presented accurately predicts the stiffness and slightly underestimates the strength and strain to failure response of the TBDC materials by 9.8% and 9.4%, respectively.

The reported differences can be explained by the analytical calculation input parameters. For instance, even though the fibre volume fraction was measured experimentally for the UD and the TBDC plate, it is possible that variations might exist in the plates which could affect their mechanical response. In addition, variations in the tape thickness and the interlaminar fracture toughness in modes I and II could also affect the accuracy of the predictions.

5.2. Effect of critical parameters

To understand the effect of the parameters reported in Section 5.1, a parametric study was carried out. The failure of the specimens was controlled by tape pull-out and therefore the two critical parameters for tape pull-out are the mode II fracture toughness of the thin plies and the thickness of the tape (Eq. (13)). The mode II interlaminar fracture toughness was varied from the measured value of 500 J/m^2 to a maximum of 1100 J/m^2 which is a typical value found in composites used in aerospace applications. Fig. 11a plots the strain to failure of the three competing mechanisms versus the orientation of the tapes for the different values of mode II fracture toughness. Fig. 11b shows a close-up of the pull-out failure strain against the tape orientations for larger angles.

It can be seen from Fig. 11 that increasing the mode II interlaminar fracture toughness from the relatively low value of 500 J/m^2 to a more standard value of 1100 J/m^2, would lead to an increase in the failure strain of the TBDC by 48%, and reaching a strain to failure close to 1.5%. It is worth noting however that this value might be reduced due to an early activation of the longitudinal tape fracture damage mechanism as seen in the UD case. All three damage mechanisms were influenced from this change but once again, according to the predictions, the damage was controlled by pull-out of tapes at an angle of about 62° to the load

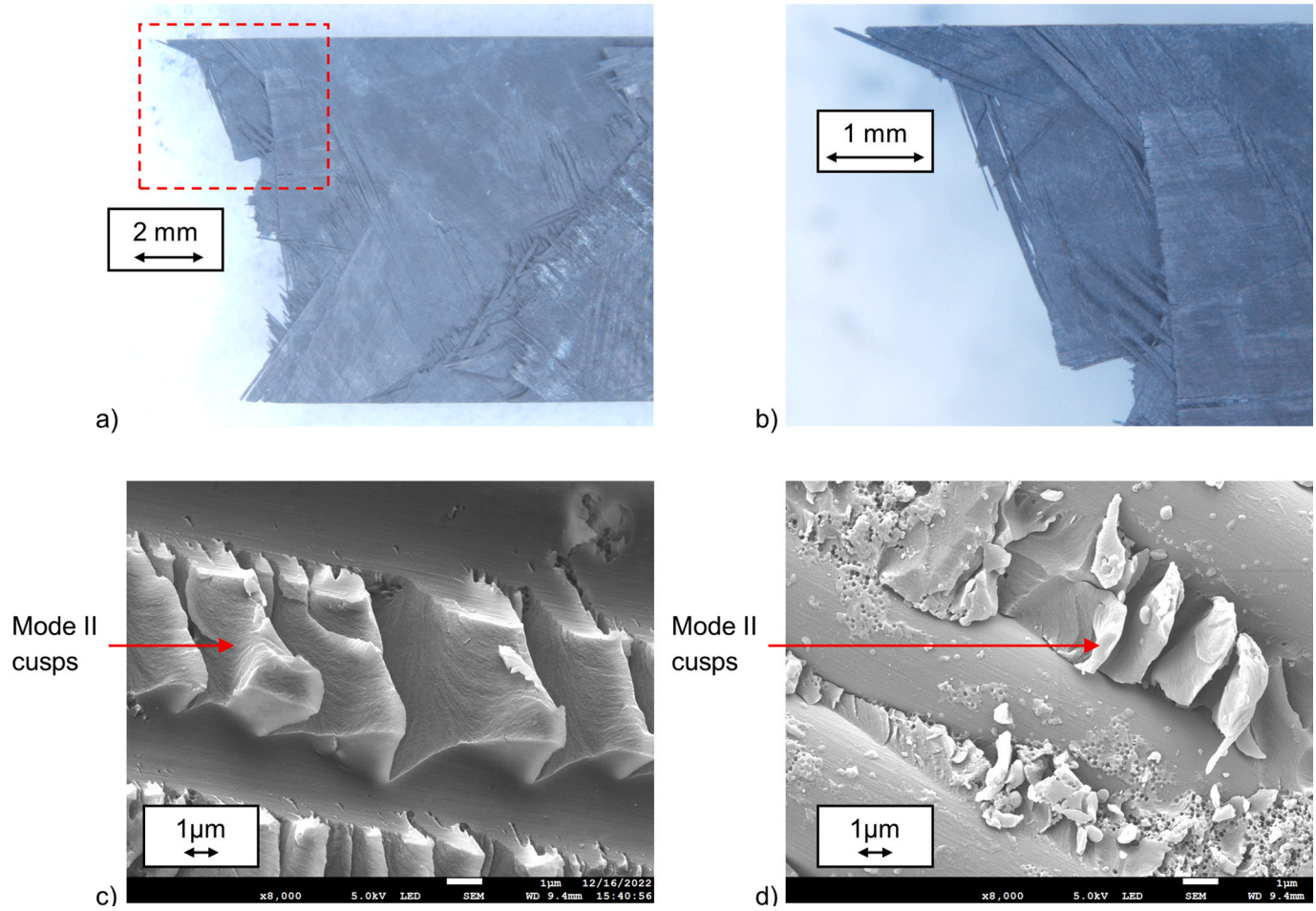

Fig. 9. Macroscopic failure of the TBDC specimens as captured with an optical microscope at a) × 5 magnification and b) × 20 magnification and shear cusps detected on the delamination interface of the c) ELS and d) TBDC specimens using SEM (× 8000 magnification).

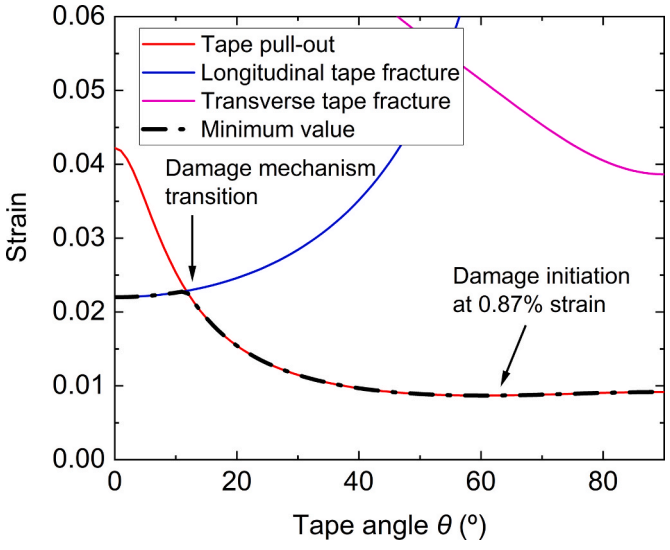

Fig. 10. Strain to failure as a function of the tape orientation angle for the TBDC tensile specimen.

direction.

Similarly, the effect of the tape thickness was investigated. For the experimental part of this project ultra-thin tapes were used and therefore this parametric study only considered thicker tapes. The thicknesses range from a minimum of 0.0214 mm to a maximum of 0.1 mm. Fig. 12a plots the strain to failure of the three competing mechanisms versus the orientation of the tapes while Fig. 12b shows a close-up of the pull-out failure strain against the tape angle.

Fig. 12 shows the beneficial effect that the thin tape has on the performance of the TBDC material. Once again, all three damage mechanisms are significantly influenced, and the most significant effect can be found in the transverse tape fracture. However, once again, the most limiting damage mechanism is due to tape-pull out and thus this will control the failure. Increasing the thickness of the tape about 5 times leads to a decrease of about 54% in the strain to failure of the TBDC.

Table 2
Experimental observations and analytical predictions of the tensile response of the TBDC specimens.

	Stiffness (GPa)	Poisson's ratio	Strength (MPa)	Strain to failure	Failure mechanism
Experimental	69.9 ± 3.2	0.363 ± 0.043	674 ± 49	0.96 ± 0.10	Tape pull-out
Analytical	70	0.331	608	0.87	Tape pull-out
Difference	0.1%	8.9%	9.8%	9.4%	

5.3. Strength comparison with TBDC systems

Table 3 provides characteristic values of the stiffness and tensile

strength of TBDCs which have been reported in the literature. The table presents the highest average value reported in each study. It is highlighted that both the stiffness and strength reported in this study exceed any other reported value. This was predicted in an earlier paper by the authors [4] where it was shown that the combination of thin tapes and high fibre modulus could potentially lead to significantly increased TBDC strengths. However, the manufacturing methods did not allow sufficient fibre volume fractions to be achieved. The present study combined the thin tapes and the high fibre modulus with high fibre volume fractions (measured as 59.4%) leading to the highest reported tensile strength of TBDC materials despite the relatively low mode II fracture toughness. It is speculated that the main differences allowing the higher fibre volume fractions to be achieved are related to the use of pre-impregnated tapes (unlike in Ref. [4] where resin films were used), the higher moulding pressure and the higher thickness of the specimens.

5.4. Conclusions

The main conclusions are summarised as follows:

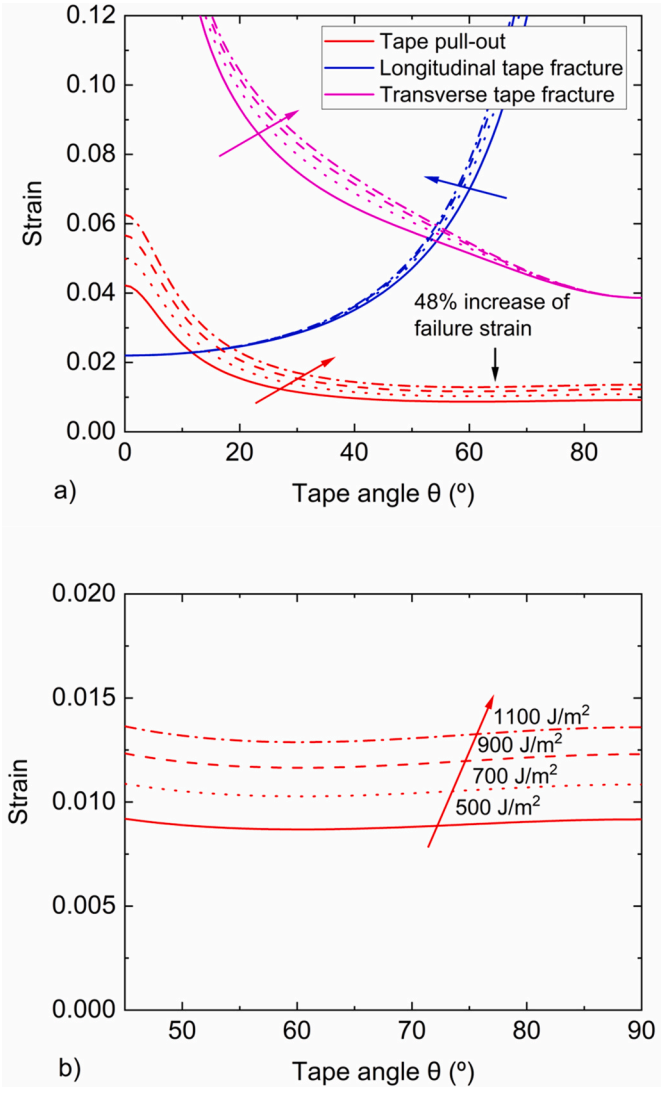

Fig. 11. a) Strain to failure as a function of the tape angle for different values of the mode II fracture toughness and b) detail for the tape pull-out strain. The four values considered were 500, 700, 900, 1100 J/m^2. The arrows indicate the effects of increasing the fracture toughness.

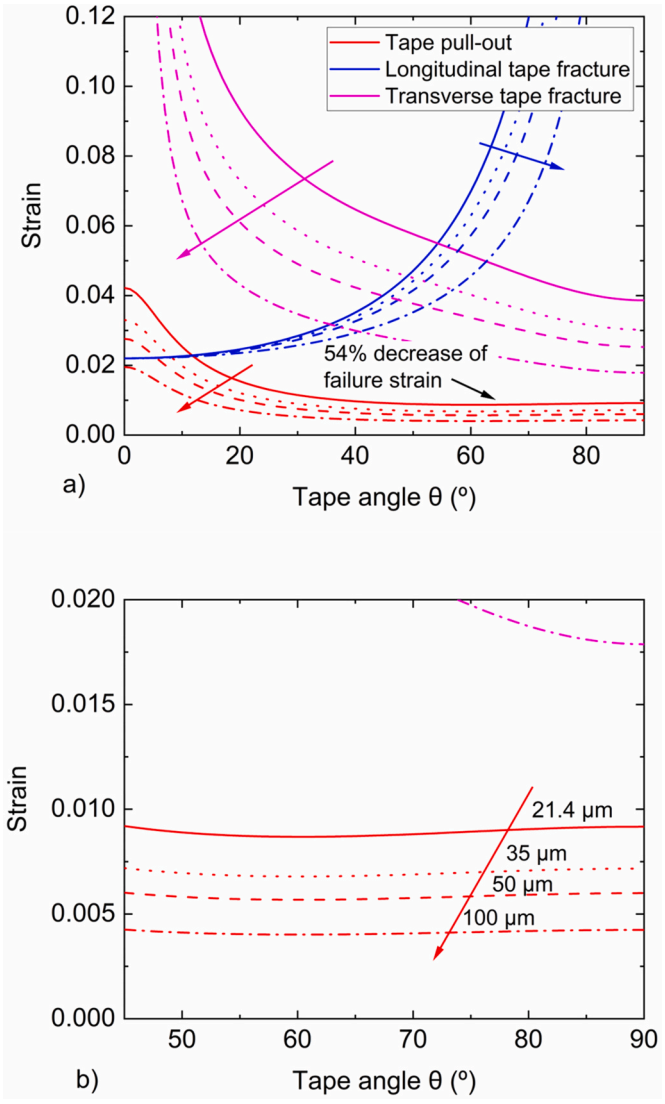

Fig. 12. a) Strain to failure as a function of the tape angle for different values of the tape thickness and b) detail for the tape pull-out strain. The four values considered were 0.0214, 0.035, 0.05, 0.1 mm. The arrows indicate the effects of increasing the tape thickness.

Table 3
Comparison of the tensile strength and stiffness of the TBDC material presented in this study compared to similar materials reported in the literature.

	Strength (MPa)	Stiffness (GPa)
Current study	**674**	**70**
Wan and Takahashi [1]	400	35
Wan and Takahashi [2]	520	50
Alves et al. [4]	300[a]	120[a]
Alves et al. [4]	600[a]	90[a]
Chen et al. [6]	200	42
Li et al. [9]	290	43
Feraboli et al. [20]	400	48
Sommer et al. [21]	381	57
Kravchenko et al. [22]	229	39

[a] Normalised values to 59% fibre volume fraction.

- A complete framework for the experimental characterisation of thin-ply TBDC materials is presented. The study characterises the tape properties by performing tensile testing (in the longitudinal and transverse directions) on UD specimens, measures the mode II fracture toughness of the thin-ply tapes, measures the stiffness and

strength response of the TBDC materials and characterises the damage mechanisms observed using SEM.

- A complete analytical method is presented which predicts the stiffness response of the TBDC materials by utilising the assumptions of the Equivalent Laminate Theory. The analytical work also proposes three competing damage mechanisms which lead to TBDC failure, namely, longitudinal and transverse tape fracture and tape-pull out. While the developed analytical tool cannot account for preferred fibre orientations nor spatial variability [8], it can provide a quick evaluation tool for the performance of the TBDC materials and their microstructural design (e.g. selection of tape thickness given the value of G_{IIc}).
- Tape pull-out is identified as the most critical damage mechanism, which causes failure of the TBDC materials, and was demonstrated by a) the analytical/experimental results comparison and b) the SEM analysis which shows clear evidence of shear deformation of the resin.
- A parametric study highlights the importance of mode II fracture toughness and tape thickness in the performance of the TBDC material. It was shown that increasing the mode II fracture toughness to more typical values for aerospace applications can lead to very significant strength improvements.
- The measured strength of the TBDC material examined in this study exceeds by about 30% any other value reported in the literature for similar TBDC materials and therefore displays the significance of combining high fibre modulus with thin tapes and optimised manufacturing methods.
- It was demonstrated that the use of pre-impregnated tapes (as opposed to infusing with resin films) and higher moulding pressure led to significantly higher fibre volume fractions and therefore TBDC strength. The presented methodology is better suited for applications where high fibre volume fractions are achieved and tape flow is restricted.

Author statement

Ioannis Katsivalis: Conceptualization, Methodology, Investigation, Formal Analysis, Software, Data curation, Writing – original draft.

Mattias Persson: Methodology, Software, Writing – review & editing.

Marcus Johansen: Methodology, Writing – review & editing.

Florence Moreau: Resources, Writing – review & editing.

Erik Kullgren: Resources, Writing – review & editing.

Monica Norrby: Investigation, Writing – review & editing.

Dan Zenkert: Conceptualization, Funding acquisition, Supervision, Methodology, Writing – review & editing.

Soraia Pimenta: Conceptualization, Funding acquisition, Supervision, Methodology, Writing – review & editing.

Leif E. Asp: Conceptualization, Funding acquisition, Supervision, Methodology, Formal Analysis, Writing – original draft.

Declaration of competing interest

The authors declare that they have no known competing financial interests or personal relationships that could have appeared to influence the work reported in this paper.

Data availability

Data will be made available on request.

Acknowledgements

The authors would like to acknowledge funding from VINNOVA (The Swedish Innovation Agency) for the Fatresfeet project (dnr. 2021–04048) and the Swedish Energy Agency via its Competence Centre Technologies and innovations for a future sustainable hydrogen economy (TechForH2, dnr. 2021–036176).

Appendix A. Supplementary data

Supplementary data to this article can be found online at https://doi.org/10.1016/j.compscitech.2023.110342.

References

[1] Y. Wan, J. Takahashi, Tensile and compressive properties of chopped carbon fiber tapes reinforced thermoplastics with different fiber lengths and molding pressures, Compos. Appl. Sci. Manuf. 87 (2016) 271–281.
[2] Y. Wan, J. Takahashi, Tensile properties and aspect ratio simulation of transversely isotropic discontinuous carbon fiber reinforced thermoplastics, Compos. Sci. Technol. 137 (2016) 167–176.
[3] S. Yamashita, T. Sonehara, J. Takahashi, K. Kawabe, T. Murakami, Effect of thin-ply on damage behaviour of continuous and discontinuous carbon fibre reinforced thermoplastics subjected to simulated lightning strike, Compos. Appl. Sci. Manuf. 95 (2017) 132–140.
[4] M. Alves, D. Carlstedt, F. Ohlsson, L.E. Asp, S. Pimenta, Ultra-strong and stiff randomly-oriented discontinuous composites: closing the gap to quasi-isotropic continuous-fibre laminates, Compos. Appl. Sci. Manuf. (2020) 132.
[5] Y. Wan, J. Takahashi, Development of carbon fiber-reinforced thermoplastics for mass-produced automotive applications in Japan, J. Compos. Sci. 5 (3) (2021) 86. https://doi.org/10.3390/jcs5030086.
[6] Z. Chen, H. Tang, Y. Shao, Q. Sun, G. Zhou, Y. Li, H. Xu, D. Zeng, X. Su, Failure of chopped carbon fiber Sheet Molding Compound (SMC) composites under uniaxial tensile loading: computational prediction and experimental analysis, Compos. Appl. Sci. Manuf. 118 (2019) 117–130.
[7] Y. Li, Z. Chen, L. Su, W. Chen, X. Jin, H. Xu, Stochastic reconstruction and microstructure modeling of SMC chopped fiber composites, Compos. Struct. 200 (2018) 153–164.
[8] M. Alves, L.M. Martulli, M. Kerschbaum, Y. Swolfs, S.V. Lomov, S. Pimenta, A 3D finite element stochastic framework for the failure of tow-based discontinuous composites, Compos. Sci. Technol. 232 (2023), 109846.
[9] Y. Li, S. Pimenta, J. Singgih, S. Nothdurfter, K. Schuffenhauer, Experimental investigation of randomly-oriented tow-based discontinuous composites and their equivalent laminates, Compos. Appl. Sci. Manuf. 102 (2017) 64–75.
[10] S. Pimenta, P. Robinson, An analytical shear-lag model for composites with 'brick-and-mortar' architecture considering non-linear matrix response and failure, Compos. Sci. Technol. 104 (2014) 111–124.
[11] C. Furtado, R.P. Tavares, A. Arteiro, J. Xavier, P. Linde, B.L. Wardle, P.P. Camanho, Effects of ply thickness and architecture on the strength of composite sub-structures, Compos. Struct. 256 (2021), 113061.
[12] J. Galos, Thin-ply composite laminates: a review, Compos. Struct. 236 (2020), 111920.
[13] Y. Li, S. Pimenta, Development and assessment of modelling strategies to predict failure in tow-based discontinuous composites, Compos. Struct. 209 (2019) 1005–1021.
[14] ASTM, D3039/D3039M – 17, Standard Test Method for Tensile Properties of Polymer Matrix Composite Materials, ASTM International, West Conshohocken, PA, 2017.
[15] ISO, ISO 15114:2014 Fibre-Reinforced Plastic Composites. Determination of the Mode II Fracture Resistance for Unidirectionally Reinforced Materials Using the Calibrated End-Loaded Split (C-ELS) Test and an Effective Crack Length Approach, British Standards International, London, 2014.
[16] M. Juntti, L.E. Asp, R. Olsson, Assessment of evaluation methods for the mixed-mode bending test, J. Compos. Technol. Res. 21 (1999) 37–48.
[17] ASTM, ASTM D3171, Standard Test Methods for Constituent Content of Composite Materials, ASTM International, West Conshohocken, PA, 2015.
[18] Z. Hashin, Failure criteria for unidirectional fiber composites, J. Appl. Mech. 47 (1980) 329–334.
[19] P.P. Camanho, C.G. Dávila, S.T. Pinho, L. Iannucci, P. Robinson, Prediction of in situ strengths and matrix cracking in composites under transverse tension and in-plane shear, Compos. Appl. Sci. Manuf. 37 (2006) 165–176.
[20] P. Feraboli, E. Peitso, F. Deleo, T. Cleveland, P.B. Stickler, Characterization of prepreg-based discontinuous carbon fiber/epoxy systems, J. Reinforc. Plast. Compos. 28 (2008) 1191–1214.
[21] D.E. Sommer, S.G. Kravchenko, B.R. Denos, A.J. Favaloro, R.B. Pipes, Integrative analysis for prediction of process-induced, orientation-dependent tensile properties in a stochastic prepreg platelet molded composite, Compos. Appl. Sci. Manuf. 130 (2020), 105759.
[22] S.G. Kravchenko, D.E. Sommer, B.R. Denos, A.J. Favaloro, C.M. Tow, W.B. Avery, R.B. Pipes, Tensile properties of a stochastic prepreg platelet molded composite, Compos. Appl. Sci. Manuf. 124 (2019), 105507.